Materials Advances

ROYAL SOCIETY OF CHEMISTRY

PAPER

View Article Online
View Journal | View Issue

Cite this: *Mater. Adv.*, 2024, 5, 3472

Photoluminescence and antibacterial performance of sol–gel synthesized ZnO nanoparticles

Mahendra Singh Rathore,*[a] Harshita Verma,[a] Sonal B. Akhani,[a] Jaivik Pathak,[a] Unnati Joshi,[b] Anand Joshi,[c] Chander Prakash,*[d] Kirtanjot Kaur[e] and Ankit Oza[cf]

The antibacterial performance and photoluminescence emission properties of ZnO nanoparticles have been investigated. The ZnO nanoparticles were synthesized using the sol–gel method, and subsequently, the sample was dried overnight at 100 °C and further annealed in air atmosphere at 350 °C for crystallization. The crystalline hexagonal phase of ZnO NPs was formed, as confirmed by X-ray diffraction results, and the obtained crystallite size was around 21 nm. The vibrational band of the prepared sample was examined using Fourier transform infrared spectroscopy. The crystalline ZnO nanoparticles exhibit an optical band gap of around 3.01 eV. The surface morphology of the sample was examined from SEM images and the phase purity was studied with EDS measurement. A strong band of PL emission was exhibited from the as-prepared sample in the visible region (512 nm). In contrast, after annealing, a PL emission band around 468.9 nm in the blue region was observed. Structural defects from the ZnO NPs may enhance PL emission properties. The antibacterial activity of synthesized sample was studied with the disc-diffusion method against *Bacillus subtilis*, *Escherichia coli* and *Pseudonomas* bacteria. Inhibition zones against bacteria were observed to be around 20 mm, 30 mm and 10 mm against *E. coli*, *B. subtilis* and *Pseudonomas* bacteria, respectively. Pure crystalline ZnO NPs were observed to be a more effective antibacterial agent against *B. subtilis* (gram-positive) bacteria compared to *E. coli* and *Pseudonomas* bacteria (gram-negative). The characteristic properties of PL emission in the visible region along with the effective antibacterial performance of the ZnO nanoparticles under an ambient light atmosphere are discussed, which have existing practical applications as a biomaterial and luminescent material.

Received 8th December 2023,
Accepted 27th February 2024

DOI: 10.1039/d3ma01096a

rsc.li/materials-advances

1. Introduction

Metal oxides have been of great and remarkable interest in many scientific fields because of their unique properties. Among these, zinc oxide (ZnO) is considered the most important due to its high thermal stability, higher band gap of 3.3 eV, and high transparency,[1,2] which makes ZnO a promising material in the fields of optoelectronics, catalysts, gas sensors, thin film based electro-optic and electronic devices, solar cells, and antibacterial agents, although the remarkable properties of ZnO show some limitation for longer use. For a decade, researchers have focused on the stochiometrically pure hexagonal phase of ZnO nanoparticles with a higher band-gap.[2–4] The engineering of the band gap is the key factor in modifying properties at the nanoscale for desired applications in optoelectronics. ZnO nanomaterials have also been attractive because of their remarkable importance in the fields of optoelectronics, nano-electronics and sensing devices,[5–7] and their biocompatible behavior also allow their use in antibacterial, antifungal, anticancer activities and as an antioxidant.[8] The modification of nanoparticles enhances their properties.[9] It has also been reported that doping may also increase antibacterial activities. Antibacterial performance depends on the physiochemical properties of NPs that may be modified by doping with metal ions.[10] The performance of NPs also depends on the surface area and surface defects, which may introduced by the dopant material and post-treatment that are responsible for the enhancement in the properties of NPs.[10–12]

An enhancement in properties without any change in the structural properties of the host matrix has significant importance. It has been reported that doping and other treatments

[a] *Department of Physics (Applied Science), Parul University, Vadodara, Gujarat 391760, India. E-mail: mahendra.rathore8944@paruluniversity.ac.in, verma.harshita98@gmail.com, sonal.pujara@paruluniversity.ac.in, jaivik.pathak11823@paruluniversity.ac.in*
[b] *Department of Mechanical Engineering, Parul University, Vadodara, Gujarat 391760, India. E-mail: unnatiajoshi@gmail.com*
[c] *Department of Mechatronics, Parul University, Vadodara, Gujarat 391760, India. E-mail: anandyjoshi@gmail.com, ankitoza6060@yahoo.in*
[d] *Centre of Research Impact and Outcome, Chitkara University, Rajpura-140401, Punjab, India. E-mail: chander.mechengg@gmail.com*
[e] *University Centre for Research and Development, Chandigarh University, Mohali 140413, India*
[f] *Chitkara Centre for Research and Development, Chitkara University, Himachal Pradesh-174103, India*

may also enhance the properties of ZnO nanomaterials without any changes in the structural unit, and they may also be capable of improving the quality of the nanomaterials.[13,14] Annealing treatment and synthesized parameters are also key factors in enhancing the properties with the achievement of stoichiometry and a pure phase of crystalline nanomaterials. Recently various synthesis methods, such as the sol–gel method, the low-temperature hydrothermal method and chemical solution methods have been adopted for ZnO nanomaterials.[15–19] Among various techniques, the sol gel technique is the preferred and most important technique in terms of cost-effectiveness.[7,20,21] The other benefit of a sol–gel approach is controlling growth and reaction parameters, which can also help to alter the properties of nanomaterials.[22] During the synthesis process, stirring time for solution preparation, pH value and ambient conditions play crucial roles in modifying the phase structure and properties of nanomaterials.[7]

The advantage of zinc oxide for use as an antimicrobial agent has been highlighted because of its relation with antimicrobial activities. The unique properties of ZnO, such as higher stability, lower toxicity and lower microbial resistance, make it a remarkably significant and important material for antibacterial agents.[23,24] The antibacterial activity against gram-positive and gram-negative microorganisms depends on the characteristic properties of the nanoparticles. The long shelf life and effective action against microorganisms and pathogens such as bacteria and fungi offered by ZnO nanoparticles have also been used in antibacterial and surface disinfectant materials. The mechanism of antibacterial activity against bacteria depends on reactive species that may be capable of damaging the bacterial wall. ZnO nanoparticles, despite the adaption of bacteria, may be capable of damaging cell membranes and interacting with proteins and DNA. This makes them important as disinfection and antimicrobial agents. The reactive oxygen species of the non-metal (ZnO) material cause an expressed change in genes, resulting in resistance being achieved over time by an induced defence mechanism.[25] For microorganisms, gram-negative bacteria are less susceptible than gram-positive bacteria to ZnO nanoparticles. The unique cell wall structure of gram-negative bacteria makes it slightly more resistant, and they have an extra outer membrane in their wall cell in contrast to gram-positive bacteria that are full of lipopolysaccharides. To better understand and create efficient antibacterial methods, researchers are actively exploring the mechanisms of action and adaptability of these metal-based nanoparticles.[26]

However, there are no systematic reports that investigate the correlation between antibacterial activities and PL emission property with the structural properties of the as-prepared and hexagonal phase of the ZnO nanoparticles.

Therefore, we have been investigating the effects of annealing on the crystallization of ZnO to enhance its structural properties, PL emission and antibacterial performance against bacteria (gram-positive and gram-negative). The ZnO nanoparticles have been synthesized using the sol–gel method followed by annealing. The PL emission properties were obtained, and the antibacterial performance has been examined against *E. coli*, *B. subtilis* and *Pseudonomas* bacteria using the disc-diffusion method. The inhibition zone represents the effects of nanoparticles on bacteria for use as an indicator of antibacterial agent performance. The possible mechanics of antibacterial activity and variation in the properties of the ZnO NPs are discussed in detail.

2. Experimental details

2.1. Materials and method

The materials were zinc acetate dihydrate (purchased from Remi-chem with purity 99%), deionized water, NaOH solution, and isopropanol. Analytical-grade chemicals were acquired and

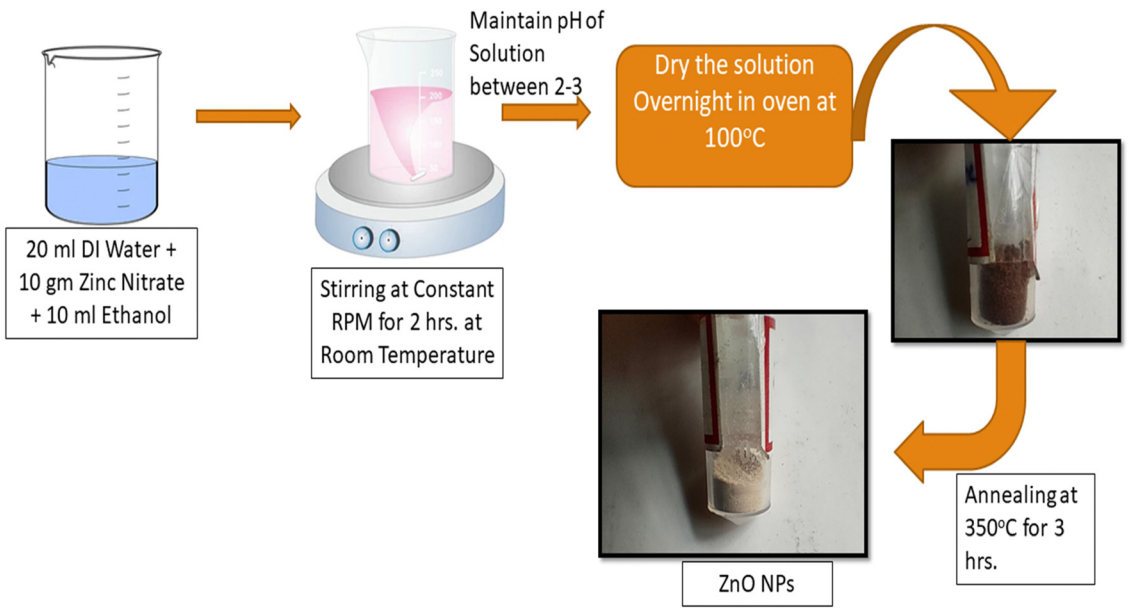

Fig. 1 Schematic diagram of the synthesis of the ZnO NPs using the sol–gel technique.

used without additional purification for the synthesis. The sol–gel synthesis method was used for the synthesis of the ZnO nanoparticles. Fig. 1 depicts a schematic diagram of the synthesis of the ZnO NPs.

2.2. Preparation of the ZnO nanoparticles

The sol–gel method was used for the synthesis of the ZnO NPs, in which a solution was prepared with a stoichiometric amount of 20 g of zinc acetate dihydrate dissolved in 50 mL of deionized water under continuous stirring for 1 hour to obtain a uniform solution of zinc acetate. After that, a few drops of NaOH solution were dissolved dropwise in the zinc acetate solution and stirred to maintain the pH at around 3. A further 30 mL of isopropanol was added dropwise and stirring was continued until a transparent solution was obtained. The prepared homogenous solution was kept overnight for 100 °C and further kept in an oven at 100 °C for 48 hours to dry the sample. Eventually, the as-calcined (dried) sample was annealed at 350 °C for 4 hours in a furnace under an ambient air atmosphere, to achieve the crystalline phase of ZnO.

2.3. Characterization

Subsequently, as-prepared and annealed ZnO nanoparticles were examined by an X-ray diffractometer (PANalytical powder XRD) using a Cu-K_α source of radiation of wavelength (λ) 1.5406 Å to examine the structural properties. FTIR spectroscopy was used to determine different vibration bands. A UV-visible spectrometer was used to analyze the optical band gap and optical transmittance property of the samples. FESEM (Nano NOVA) was used to analyze the SEM images and EDS spectra of the ZnO nanoparticles. The photoluminescence (PL) emission properties of the synthesized samples were studied with an FL spectrometer. The PL emission was measured by excitation of wavelength at 325 nm in the UV to visible region.

2.4. Antibacterial activity

The antibacterial activity was evaluated using the disc-diffusion method, of the as-prepared and annealed ZnO NPs. The antibacterial activity was examined against gram-positive (*B. subtilis*) and gram-negative (*E. coli* and *Pseudomonas*) microorganisms. For the antibacterial test, all microorganism cultures were first prepared from fresh broth culture which was kept overnight at 35 °C. Muller-Hinton broth was used for cultivation of bacterial microbes, at 35 °C in an incubator at 150 rpm for 24 hours. Each strain of microbe was adjusted for bacterial suspension, to a concentration that was nearly equal to McFarland's standard turbidity (3×10^8 bacteria per mL). The microbial culture was arranged on nutrient-dense agar plates, by dispersion of the culture broth. Sterile Whatman paper discs impregnated with a nanoparticle solution of ZnO were deposited on the culture medium surface. The discs were permitted to stand for absorption of the culture. For *E. coli* and *B. subtilis*, holes were made in the culture medium on set agar containing bacteria. The inhibition zone area of the disc was used to evaluate the antibacterial performance of the ZnO nanoparticles.

3. Results and discussion

3.1. XRD analysis

Structural properties and phase identification were studied with an X-ray diffractometer. The XRD patterns of the samples were recorded by the interaction of Cu-Kα radiation scattered at scattering angles ranging from 20° to 70° and are shown in Fig. 2. The XRD results reveal that the as-prepared calcined dried powder shows a crystalline phase along with mixed impurities, whereas after annealing at 350 °C, the other impurity-related peaks have disappeared from the XRD pattern. The pure hexagonal crystalline phase of the ZnO nanoparticles was observed after annealing. The absence of all other peaks corresponding to impurities indicates the nucleation and growth of the pure hexagonal phase of the ZnO nanoparticles, which was confirmed by the presence of XRD peak positions at scattering angles corresponding to (100), (002). (101), (102), (110), (103), (200), (112) and (201) planes that strongly matched JCPDS reference card no: 00-005-0664.

The XRD results demonstrate that the crystalline quality and phase structure of the ZnO nanoparticles was improved by thermal annealing. During the annealing process, because of the thermal energy provided to species, the kinetic energy of atomic species increases due to the energy gained during the thermal process.[27,28] The higher energy of atomic species might try to reorient them within the plane and place them at the preferred orientation of atomic positions, causing the growth of the crystalline hexagonal phase structure of the ZnO NPs.[28]

Scherer's formula[29] was used for the crystallite size of the ZnO NPs, which was calculated by considering the predominant major peak of plane (100), and was found to be around 21 nm.

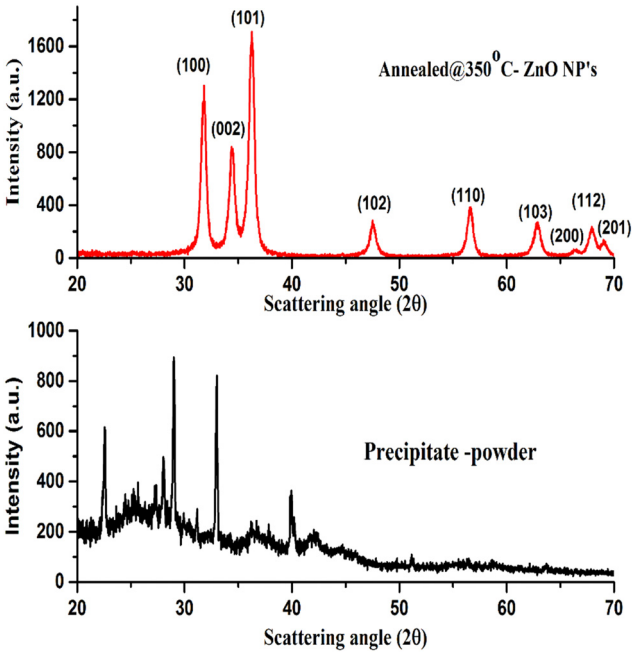

Fig. 2 XRD patterns of the as-dried (precipitate) sample and annealed ZnO NPs.

$$D = \frac{K\lambda}{\beta\cos(\theta)}$$

where D is the crystallite size, K is the shape factor ($K = 0.9$), λ is the wavelength of Cu (Kα) radiation (1.5406 Å), θ is the angle of diffraction, and β is full-width at half-maximum of the dominant diffraction peak in radians.

The lattice strain of the as-prepared ZnO NPs was calculated and found to be around 2.32×10^{-3}.

$$\varepsilon = \frac{\beta}{4\tan\theta}$$

The d-spacing relation for the hexagonal structure of the ZnO NPs is given by,

$$\frac{1}{d^2} = \frac{4}{3}\left(\frac{h^2 + hk + k^2}{a^2}\right) + \frac{l^2}{c^2}$$

where a and c are the lattice parameters and d represents the inter-planar spacing corresponding to reflection planes with Miller indices (h k l). Using the plane corresponding to the predominant peak, the lattice parameters (a and c) were calculated and obtained at around 3.25 Å and 5.63 Å, respectively. The c/a ratio is obtained at around 1.7 for the hexagonal structure. The obtained values of the lattice parameters are in good agreement with the reported standard data file (card no. 00-005-0664). The c/a ratio represents the perfect hexagonal structure of ZnO. Thus, the XRD patterns confirmed that the as-calcined dried sample was impure with a mixed phase, whereas annealing removes the impurities, and the pure hexagonal phase of the ZnO nanoparticles is obtained.

3.2. FTIR measurements

The presence of functional and vibrational groups along with the chemical structure of the prepared samples were observed using FTIR spectroscopy. The IR spectra measured in the wavenumber range from 500 to 1600 cm^{-1} of as-calcined dried and annealed ZnO NP samples are shown in Fig. 3. It was found that small intense IR bands were observed in the calcined (dried) powder sample; however, after annealing, a sharp intense band appeared in the IR spectra of annealed ZnO. The band position was observed within the range from 500 to 600 cm^{-1} centered around 555 cm^{-1}, corresponding to the Zn–O stretching vibration band of the hexagonal phase structure of ZnO NPs.[30] The result implies that after annealing the samples become crystalline and exhibit the hexagonal phase of ZnO. IR results complement the results obtained from XRD.

In addition, an IR band is observed in the region between 662 cm^{-1} and 878 cm^{-1}, attributed to stretching of the Zn–O bond.[31] Further peaks at 1139 cm^{-1} and 1350 to 1420 cm^{-1} may be ascribed to –C–O–C– and C–O stretching modes and bending of the hydroxyl residue (O–H group) because of atmospheric moisture.[32] The intensity of C–O and O–H group related peaks decreased after annealing, which indicates that thermal annealing improved the crystalline quality of the ZnO NPs.

3.3. UV-Vis-NIR spectroscopy

The ZnO nanoparticles were characterized using UV-visible-NIR spectroscopy within the wavelength range from 400 nm to 800 nm, for measurement of optical properties. The optical transmittance spectra of ZnO samples are shown in Fig. 4. It was found that the poor transmittance exhibited in the visible region is shown in the transmittance spectra of the as-dried sample. The poor transmittance occurs due to the presence of hydroxyl and other impurities present in the as-dried sample that was also confirmed by the XRD and FTIR results, whereas after annealing of ZnO, the average transmittance changed drastically and achieved around 80% in the visible to IR region from the ZnO NPs. The improvement in the optical transmittance

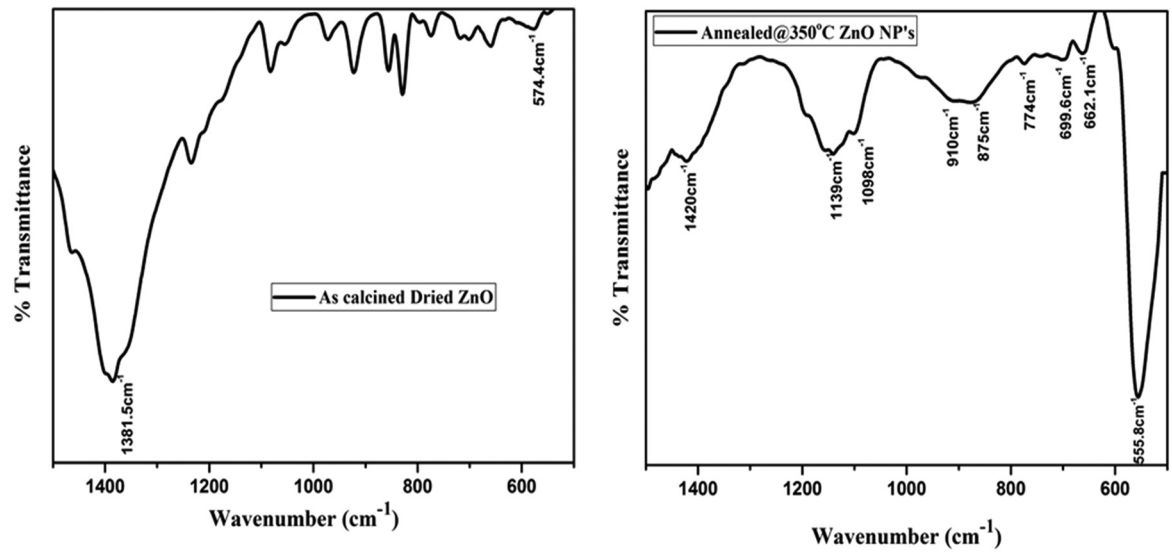

Fig. 3 IR transmittance spectra of the as-dried (as-prepared) and annealed ZnO NPs.

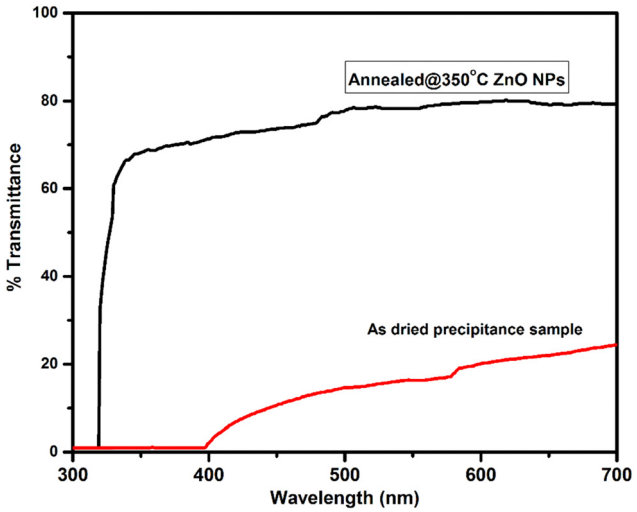

Fig. 4 Optical transmittance spectra of the ZnO NPs.

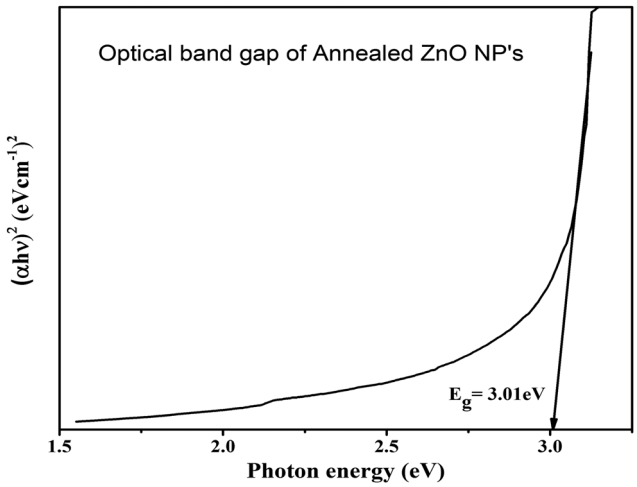

Fig. 5 Tauc plot for the optical band gap of annealed ZnO NPs.

is caused by the enhancement in the crystalline quality of the sample. This implies that the better crystallinity and quality of the nanomaterials show good optical properties.[33,34]

The Tauc's plot was used to calculate the optical band gap of the synthesized nanoparticles. The Tauc relation[35] is,

$$(\alpha h\nu) = A(h\nu - E_g)^m,$$

where α is the coefficient of absorption, $h\nu$ is the energy of an incident photon, A is a constant and m shows the allowed/forbidden electronic transitions (where a direct transition is considered to have $m = 1/2$).

The intercept of the linear portion with the X-axis (energy value) in extra plotting between $(\alpha h\nu)^2$ *vs.* photon energy (E) is represented in Fig. 5. The optical band gap energy of the samples was evaluated by a better fit of $(\alpha h\nu)^2$ against the photon energy (E). It was found that the optical band gap of the annealed ZnO NPs is obtained at around 3.01 eV. The obtained result was approximately equal to the reported direct band gap (3.37 eV) of the hexagonal phase of the ZnO nanoparticles. The calculated band gap of ZnO depends on the impurities, crystalline quality and size of nanostructures. The calcination temperature played a crucial role in modifying the quality of ZnO. With the annealing temperature, the kinetic energy was not enough to agglomerate them again in the lattice, which may be responsible for oxygen vacancies in the crystal structure. Due to oxygen-related defects in ZnO, the optical band gap was slightly down compared to the reported band gap of hexagonal ZnO nanoparticles.

3.4. Surface morphology and EDS measurement

The surface morphology of the prepared samples was investigated using SEM images and is shown in Fig. 6. The particles appeared and were agglomerated on the surface of the as-pristine sample, as confirmed by the SEM image. However, after annealing, spherical and dense particles were observed that were uniformly distributed on the surface. The particles were formed with bigger size and were non-spherical as confirmed from the image of the annealed sample. A bigger edge of the particles appeared due to thermal annealing that may be responsible for the crystallization of ZnO. This exhibits a greater surface area and possesses a strong and lasting affinity towards the particles. Thus, this implies that the stability of the nanoparticles and their agglomeration were influenced by sintering factors.

The elemental composition in the annealed sample was examined using EDS measurement during the FESEM analysis and is shown in Fig. 7. It was found that the annealed ZnO sample is free from impurities and represents the growth of the pure phase of ZnO nanoparticles. In the spectra, the predominant peaks observed at 1 keV and ~8.6 keV correspond to the distinct and predominant peaks of the zinc element. In addition, the singular peak observed at around 0.5 keV indicates the presence of oxygen element. The positions of the peaks corresponding to Zn and O demonstrate the growth of high-purity ZnO nanoparticles. The intensity of the peak is relevant to the atomic weight% of the presence of the element in the molecule. It was found that the samples possess 98.37 zinc wt% associated with 1.67 oxygen wt%. The inset of Fig. 7 indicates the elemental composition and atomic wt% of Zn and O in the synthesized ZnO sample. Thus, EDS results confirm the pure phase of ZnO NPs, which is complementary to the XRD results of the annealed ZnO sample.

3.5. Photoluminescence

The spectra of the PL emission of the prepared samples were recorded from excitation with wavelength of 325 nm at room temperature. The excitation energy of 325 nm (3.81 eV) used is higher than the energy band gap of ZnO (3.1–3.4 eV), so an electron may jump easily for excitation from the valance to the conduction band. Fig. 8 represents the PL spectra of as-prepared and annealed samples. An intense broad PL emission band was exhibited at around 511.7 nm in the visible region in the PL spectrum of the as-dried sample. In addition, small PL bands near to the edge in the near-UV and violet region at

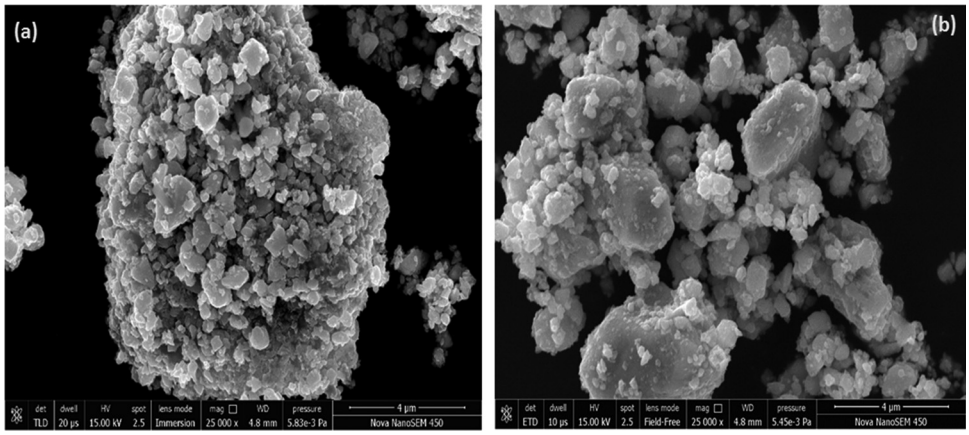

Fig. 6 SEM images of the ZnO nanoparticles (a) as-prepared and (b) annealed.

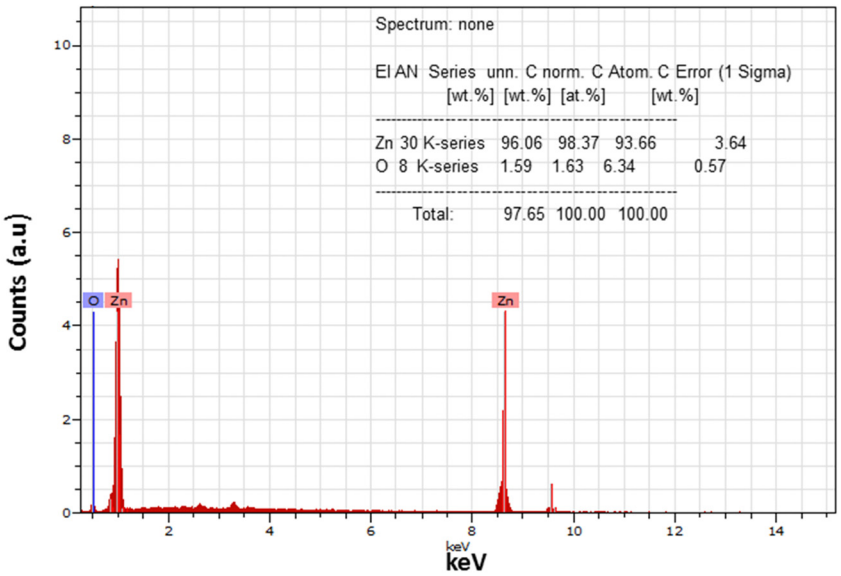

Fig. 7 EDS spectra of annealed ZnO samples.

around 365.6 nm and 406.8 nm, respectively, were also exhibited by the as-prepared sample. The PL emission band close to the UV emission region can be attributed to the near band edge transition of ZnO and occurred because of the radiative recombination of free excitons.[17,30] Green PL emission centered at 511.7 nm (2.64 eV) came from the as-prepared sample. The recombination of electrons with photo-excited holes in the valence band could be responsible for the green emission. It implies that the as-prepared sample has impurity phases which represent greater availability of ionized oxygen vacancies. The rate of recombination of excited holes with ionized oxygen vacancies was higher, resulting in intense green PL emission from the as-prepared sample. The positions of various PL emission bands exhibited by the as-prepared and annealed ZnO NPs are listed in Table 1.

However, it is observed that after annealing, the green PL emission peak intensity decreases and exhibits a small edge. The reduction in the PL emission peak indicates the decreasing probability of the recombination of singly ionized oxygen vacancies. The probability of recombination of oxygen vacancies may also depend on the crystalline quality of the sample. Due to annealing, there is an improvement in the oxygen-related defects that may be responsible for the variation in the intensity of the PL band.[27] It was observed that the UV emission intensity increased slightly after annealing. The increase in emission implies that the possibility of recombination of free excitons increases due to thermal annealing.[12,27] During the annealing process, because of the separation of donor bond excitons into free excitons, the recombination rate is increased.

Further, it is observed that after annealing at 350 °C, an intense blue PL band is exhibited at around 468.9 nm from the crystalline ZnO NPs. The occurrence of defect levels in the ZnO sample may be responsible for the exhibition of the blue PL emission peak. The existence of a strong blue PL band from the

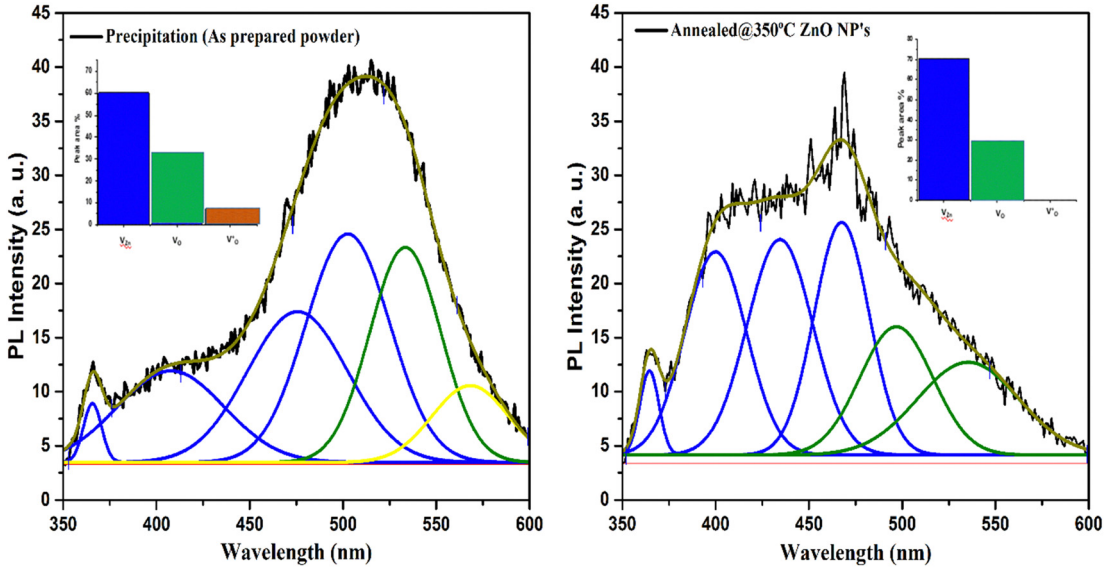

Fig. 8 Deconvoluted PL emission spectra of the as-prepared and annealed ZnO NPs. Inset: peak area % of defect levels of ZnO.

Table 1 PL emission band positions exhibited by the as-dried and annealed ZnO NPs

PL peak position of as-dried samples		PL peak position annealed@ 350 °C ZnO NPs	
(in nm)	(in eV)	(in nm)	(in eV)
365.6	3.395	364.1	3.409
406.8	3.05	400	3.10
—	—	451	2.75
		468.9	2.647
511.7	2.42	521	2.38

annealed sample indicates that the defect levels were increased in the lattice structure of hexagonal crystalline ZnO nanoparticles after annealing. Conversely, another broad PL band was observed around 400 nm within the violet region from the crystalline phase of ZnO. The position of the violet emission band is attributed to the transition of an electron from the Zn level to the valence band. This implies that annealing promotes and increases the probability of transition from the Zn level near the conduction band to the valence band, which is responsible for PL emission from the crystalline ZnO sample.[36]

The presence of defect levels or impurities and carrier charge recombination in the samples can also be evaluated from the deconvolution of PL spectra that was performed using the Gaussian distribution function.[37] Fig. 8 represents the Gaussian fitted deconvolution of PL emission spectra. In deconvoluted PL spectra, three peaks were observed in the shortened wavelength (range from 350 to 435 nm) of the as-prepared sample. The recombination of electrons of the valance band to holes in the conduction band is responsible for the peak observed at around 365 nm attributed to near band edge (NBE) emission. In contrast, the interstitial defect level in Zn was responsible for the violet emission observed around 400 nm.[38]

The violet and blue emission bands at around 435 nm and 469 nm, respectively, are found in the annealed sample, which are associated with the transition from the conduction band of ZnO or donor-defect level of Zn to acceptor-defect level of Zn vacancies (V_{Zn}) or to surface trap states. An absence of the violet emission band is found in the as-prepared sample that indicates the absence of Zn-related defects in the as-prepared ZnO. A broad visible PL emission band ranging from 470 to 535 nm is exhibited in the as-prepared sample, corresponding to the deep-level emission defects that arise due to zinc vacancies (V_{Zn}), oxygen vacancies (V_O^-) and defects in the band gap of ZnO.[39,40] A strong PL emission peak is observed at 468 nm in the annealed sample. This implies that band-gap-related defects may be removed after annealing, as was also confirmed by the XRD and UV-Vis spectroscopy results. In the deconvoluted spectra, a small intense green to yellow emission band was found at around 568 nm in the as-prepared sample, attributed to single charged oxygen vacancies (V_O^+)[41] that was absent in the annealed ZnO sample. This demonstrates that single charged oxygen vacancy related defects were absent in the pure ZnO nanoparticles. The results demonstrate that a high concentration of zinc vacancies was exhibited in the pure annealed ZnO nanoparticles.

The variation in intensity of the PL emission and PL band position also correlated with the structural property and crystalline quality of the nanomaterials.[34] Thus, it was clear that PL results show good agreement with structural results. Hence, the results show the formation of high-quality ZnO NPs due to annealing, with strong intensity of PL emission within the range of the near-UV to the visible region observed. Thus, the photoluminescence emission properties of the ZnO nanoparticles have significant importance due to strong PL emission in the near-UV and blue region that make them a suitable and appropriate material for use as host material in display devices for optoelectronics applications and white light emitting diodes.

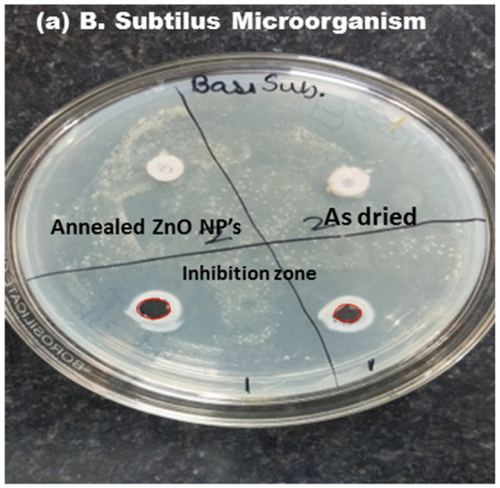

Fig. 9 Inhibition zone of the as-prepared and annealed ZnO NPs against gram-positive (*B. subtilis*) bacteria.

3.6. Antibacterial activity

The antibacterial performance of as-prepared and annealed ZnO nanoparticles was examined against gram-positive (*B. subtilis*) and gram-negative (*E. coli* and *Pseudomonas*) microorganisms using the disc-diffusion method. The inhibition zone of ZnO nanoparticles against *B. subtilis*, and *E. coli* and *Pseudomonas* bacteria are shown in Fig. 9 and 10, respectively. It was found that the as-prepared samples show a lower effect against bacteria than the annealed ZnO NPs. The inhibition zones are observed to be around 10 mm and 0.8 mm against *E. coli* and *B. subtilis* bacteria from the as-prepared ZnO sample, but there was no inhibition zone observed against *Pseudomonas*. This implies that the as-prepared nanomaterial showed antibacterial activity only against some specific bacteria. However, an annealed crystalline ZnO NP solution was more effective against all bacteria. The results indicate that the inhibition zone diameters against *B. subtilis*, *E. coli* and *Pseudomonas* are obtained at around 30 mm, 20 mm and 10 mm, respectively. Moreover, the inhibition zone diameter of gram-positive bacteria is greater than that for gram-negative microorganisms. This indicates that the crystalline pure phase of the ZnO NPs was more effective against gram-positive bacteria compared to gram-negative bacteria. The better performance of the ZnO NPs against gram-positive microorganisms is also in good agreement with reported studies.[24,42–44]

The potential reason behind the antibacterial performance can be explained by the cell wall difference between gram-negative and gram-positive bacteria. Gram-positive bacteria (*B. subtilis*) have cell walls which consist of thick peptidoglycan layer that provides a physical barrier and protects the cell. This peptidoglycan is fixed with surface proteins and teichoic and lipo-teichoic acids. Conversely, gram-negative bacteria have an additional external membrane which contains lipopolysaccharides, proteins and a thin layer of peptidoglycan.[24,26,45–47] It is difficult to damage the cells by the attack of the ZnO nanoparticles when they interact on the bacteria due to the external membrane in gram-negative bacteria. Antibacterial activity indications for the ZnO nanoparticles show that the crystalline ZnO NPs are more effective and better against gram-positive bacteria compared to gram-negative ones.

The antibacterial performance mechanism of the ZnO NPs may be the result of the dissolution of the ZnO NPs, which produces reactive oxygen species (ROS) and Zn^{2+} ions. During the interaction with bacteria, the Zn^{2+} ions reduce the metabolism and enzymatic system of amino acids, and the reactive oxygen species provide amino hydroxyl ions that are able to destroy the cell membrane component and DNA, lipids and protein.[24,48] This results in destruction of the cell wall, the ability to kill the bacteria and shows better antibacterial activity. The antibacterial performance is effected by the impurity phase of the nanoparticles.

Thus, obtained results demonstrate the formation of a crystalline hexagonal phase of ZnO after annealing. The ZNO NPs were more effective than the as-prepared samples, good agreement was established and correlation was shown between their structural, photoluminescence and antibacterial performance against bacteria. The obtained results are better than those previously reported, and a comparison between the present study and a few reported studies is tabulated in

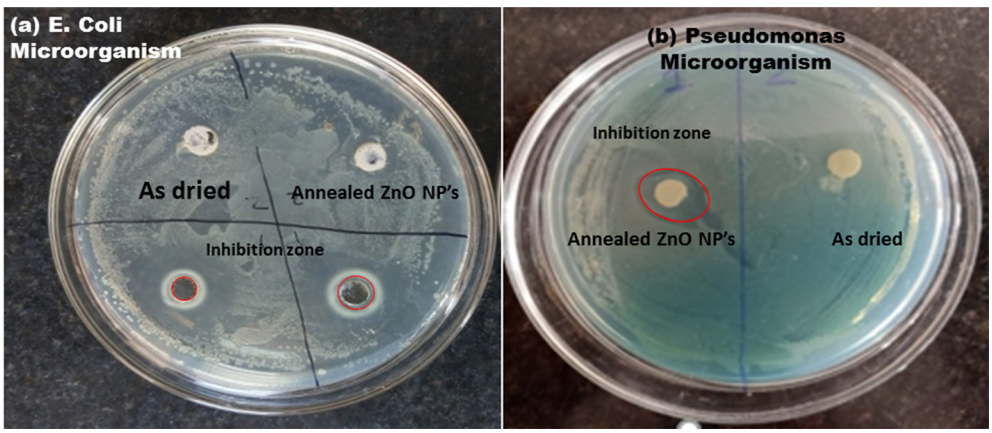

Fig. 10 Inhibition zone of the as-prepared and annealed ZnO NPs against gram-negative (a) *E. coli* and (b) *Pseudomonas* bacteria.

Table 2 Comparison of photoluminescence, optical band gap and antibacterial activity of ZnO nanoparticles with the literature

Sr. no.	Synthesis of nanoparticles	Photoluminescence emission	Antibacterial activity inhibition zone in mm	Optical band gap	Ref.
1	ZnO nanoparticles by chemical and biosynthesis	Blue (403 nm) to green (527 nm) emission	Gram-positive (9 mm for chemical synthesis 20 mm for higher concentration of ZnO by biosynthesis NPs) and gram-negative (10 mm and 21 mm)	3.02 to 3.13 eV	Nithya *et al.*[49]
2	Sr-doped ZnO nanoparticles synthesis by soft chemical method	Blue (408 nm) to green-blue (492 nm) emission	Gram-negative *E. coli* (14 mm to 17 mm)	—	Karthick *et al.*[12]
3	Co-doped ZnO nanoparticles synthesis by wet precipitance method	Week UV emission (400 nm) and green emission (507 nm)	Without sunlight *E. coli* (18 mm from pure ZnO and 22 nm zone from Co-doped ZnO)	3.28 eV (pure ZnO)	Sashi B. Rana *et al.*[21]
4	ZnO nanoparticles using facile chemical and physical method	Near-UV emission (400 nm), blue and to green (492 nm) emission	Gram-negative (*E. coli* maximum 62–72% for higher concentration 1 mg mL^{-1}) and gram-positive	—	Nataliya *et al.*[50]
5	ZnO nanoparticles using sol–gel method	Intense UV (364.1 nm), violet to blue emission (400 nm), blue emission (468.9 nm), and green emission (511 nm and 521 nm)	Gram-positive (30 mm) and gram-negative *E. coli* (20 mm) and *Pseudomonas* (10 mm)	3.01 eV	Present study

Table 2. It is observed that the results are in good agreement and show better performance against gram-positive microorganisms, and an intense blue and green PL emission is observed from the annealed ZnO nanoparticles.

Conclusion

The hexagonal phase of the ZnO NPs was synthesized using sol gel methods followed by annealing at 350 °C in air atmosphere. The effects of annealing on the structural properties and correlation with the optical, photoluminescence and antibacterial activity of ZnO NPs were investigated. The annealing enhanced the crystalline quality and removed impurities, whose results were confirmed by the XRD and FTIR spectra. The crystallite size was observed to be around 21 nm. The IR band observed in the range 500–600 cm^{-1} was attributed to the stretching vibration band of ZnO. The optical transmittance was drastically increased to around 80% after annealing. The optical band gap was obtained at around 3.01 eV. Intense UV to blue PL emission was observed from the sample. The formation of a pure phase of ZnO was examined using EDS measurement. Strong green emission was observed from the as-prepared sample, whereas the annealed sample shows strong blue PL emission at 468.9 nm and violet emission at around 412 nm. The deconvoluted PL spectra demonstrate the defect levels of the ZnO nanoparticles. The intensity of the PL band increases after annealing. The crystalline ZnO NPs show inhibition zone diameters against *B. subtilis*, *E. coli* and *Pseudomonas* of around 30 mm, 20 mm and 10 mm, respectively. The results demonstrate that the crystalline ZnO NPs show better antibacterial activity against gram-positive bacteria compared to gram-negative bacteria. The results demonstrate the correlation between the structural properties with photoluminescence emission properties in the near-UV to visible region (365 nm to 469 nm) and antibacterial performance against gram-positive and gram-negative bacteria by the ZnO NPs. The mechanisms of luminescence and antibacterial activities are of significant importance for use as antibacterial agents and are important in optoelectronic and biomaterial applications.

Conflicts of interest

There are no conflicts to declare.

Acknowledgements

We would like to acknowledge to the Dr KVR Murthy, (M S University, Vadodara, Gujarat) for PL spectroscopy and Materials Research Center – MNIT Jaipur for providing characterization facilities.

References

1 M. Kahouli, A. Barhoumi, A. Bouzid, A. Al-hajry and S. Guermazi, *Superlattices Microstruct.*, 2015, **85**, 7.

2 H. Y. Sohn and A. Murali, *Molecules*, 2021, **26**, 1456.
3 M. A. Borysiewicz, *Crystals*, 2019, **9**(10), 505.
4 R. S. Mohar, I. Sugihartono, V. Fauzia and A. A. Umar, *Surf. Interfaces*, 2020, **19**, 100518.
5 Y. Wang, Y. Yang, L. Xi, X. Zhang, M. Jia, H. Xu and H. Wu, *Mater. Lett.*, 2016, **180**, 55.
6 B. G. Shohany and A. K. Zak, *Ceram. Int.*, 2020, **46**(5), 5507–5520.
7 S. Arya, P. Mahajan, S. Mahajan, A. Khosla, R. Datt, V. Gupta, S.-J. Young and S. K. Oruganti, *ECS J. Solid State Sci. Technol.*, 2021, **10**, 023002.
8 M. Nilavukkarasi, S. Vijayakumar and S. Prathipkumar, *Mater. Sci. Energy Technol.*, 2020, **3**, 335.
9 V. Saraswathi, R. Ramanathan and R. Ramasamy, XII, 1167.
10 S. Sinha, V. Patel, H. Verma, T. K. Akhani and M. S. Rathore, *Mater. Today: Proc.*, 2022, **67**(7), 694–700.
11 M. Sajjad, I. Ullah, M. I. Khan, J. Khan, M. Y. Khan and M. Tauseef, *Results Phys.*, 2018, **9**, 1301.
12 R. Karthick, P. Sakthivel, C. Selvaraju and M. S. Paulraj, *J. Nanomater.*, 2021, **2021**, 8352204.
13 S. Liu, L. Zhu, W. Cao, P. Li, Z. Zhan, Z. Chen, X. Yuan and J. Wang, *J. Alloys Compd.*, 2021, **858**, 157654.
14 G. Kasi, K. Viswanathan, K. Sadeghi and J. Seo, *Prog. Org. Coatings*, 2019, **133**, 309.
15 R. E. Adam, H. Alnoor, G. Pozina, X. Liu, M. Willander and O. Nur, *Solid State Sci.*, 2020, **99**, 106053.
16 R. Kara, L. Mentar and A. Azizi, *RSC Adv.*, 2020, **10**, 40467.
17 S. Liu, L. Zhu, W. Cao, P. Li, Z. Zhan, Z. Chen, X. Yuan and J. Wang, *J. Alloys Compd.*, 2021, **858**, 157654.
18 R. Sagheer, M. Khalil, V. Abbas, Z. N. Kayani, U. Tariq and F. Ashraf, *Optik*, 2020, **200**, 163428.
19 K. Huang, Z. Tang, L. Zhang, J. Yu, J. Lv, X. Liu and F. Liu, *Appl. Surf. Sci.*, 2012, **258**, 3710.
20 P. Mahajan, A. Singh and S. Arya, *J. Alloys Compd.*, 2020, **814**, 152292.
21 S. B. Rana, R. P. P. Singh and S. Arya, *J. Mater. Sci. Mater. Electron.*, 2017, **28**, 2660.
22 D. Bokov, A. Turki Jalil, S. Chupradit, W. Suksatan, M. Javed Ansari, I. H. Shewael, G. H. Valiev and E. Kianfar, Nanomaterial by Sol–Gel Method: Synthesis and Application, *Adv. Mater. Sci. Eng.*, 2021, **2021**, 1–21.
23 B. Mohapatra, S. Choudhary, S. Mohapatra and N. Sharma, *Mater. Today Commun.*, 2023, **34**, 105083.
24 B. Abebe, E. A. Zereffa, A. Tadesse and H. C. A. Murthy, 2020.
25 E. N. Danial, M. Hjiri, M. S. Abdel-wahab, N. H. Alonizan, L. El Mir and M. S. Aida, *Inorg. Chem. Commun.*, 2020, **122**, 108281.
26 I. Charti, A. Azouzi, A. Belghiti, S. Sair, Y. Abboud and A. El Bouari, *Curr. Res. Green Sustainable Chem.*, 2021, **4**, 100102.
27 M. S. Rathore, A. Vinod, R. Angalakurthi, A. P. Pathak, F. Singh, S. K. Thatikonda and S. R. Nelamarri, *Appl. Phys. A: Mater. Sci. Process.*, 2017, **123**(708), 1–10.
28 M. Goswami, N. C. Adhikary and S. Bhattacharjee, *Optik*, 2018, **158**, 1006.
29 B. D. Cullity, *Elements of X-ray Diffraction*, 1978, vol. 29.
30 J. Singh, P. Kumar, K. S. Hui, K. N. Hui, K. Ramam, R. S. Tiwari and O. N. Srivastava, *CrystEngComm*, 2012, **14**, 5898.
31 L. Saikia, D. Bhuyan, M. Saikia and B. Malakar, *Appl. Catal., A*, 2014, **490**, 42.
32 G. Kasi and J. Seo, *Mater. Sci. Eng., C*, 2019, **98**, 717.
33 M. Singh and N. Srinivasa, *Adv. Sci. Lett.*, 2018, 1.
34 M. S. Rathore, A. Vinod, R. Angalakurthi, A. P. Pathak, S. K. Thatikonda and S. R. Nelamarri, *Phys. B*, 2022, **625**, 413466.
35 J. Tauc, *Amorphous Liq. Semicond.*, 1974, 159.
36 J. Pathak, S. Bharatbhai and M. Singh, *Mater. Today: Proc.*, 2024, 1.
37 M. Rocha, F. P. Araujo, S. Castro-Lopes, I. S. de Lima, E. C. Silva-Filho, J. A. Osajima, C. S. Oliveira, B. C. Viana, L. C. Almeida, Y. Guerra and R. Peña-Garcia, *Ceram. Int.*, 2023, **49**, 2282.
38 M. C. R. Silva, S. Castro-Lopes, A. G. Jerônimo, R. Barbosa, A. Lins, P. Trigueiro, B. C. Viana, F. P. Araujo, J. A. Osajima and R. R. Peña-Garcia, *Molecules*, 2024, 29.
39 A. S. Soares, F. P. Araujo, J. A. Osajima, Y. Guerra, B. C. Viana and R. Peña-Garcia, *J. Photochem. Photobiol., A*, 2024, **447**, 115235.
40 M. Costa-Silva, F. P. Araujo, Y. Guerra, B. C. Viana, E. C. Silva-Filho, J. A. Osajima, L. C. Almeida, E. Skovroinski and R. Peña-Garcia, *Mater. Chem. Phys.*, 2022, **292**, 126814.
41 A. S. Soares, F. P. Araujo and R. França, *et al.*, *J. Mater. Res.*, 2023, **38**, 2439–2452.
42 N. Talebian, S. Matin and M. Doudi, *J. Photochem. Photobiol., B*, 2013, **120**, 66.
43 J. Ghasemian, A. Khudair, F. Ezzatkhah and M. Shakibaie, *Biomed. Pharmacother.*, 2023, **164**, 114984.
44 T. Shuga, H. Elsayed, A. Mohamed and M. Maaza, *J. Phys. Chem. Solids*, 2022, **160**, 110313.
45 N. Chamkouri, N. Jomehzadeh and N. Naserzadeh, *Curr. Res. Green Sustainable Chem.*, 2023, **6**, 100366.
46 M. Alikord, N. Shariatifar, M. Saraji, G. Jahed Khaniki, H. Hosseini and M. Fazeli, *Bionanoscience*, 2023, **13**, 1036–1051.
47 H. Wu, Y. Meng, M. Yu and H. Yang, *Appl. Clay Sci.*, 2023, **242**, 107024.
48 K. Qi, B. Cheng, J. Yu and W. Ho, Review on the improvement of the photocatalytic and antibacterial activities of ZnO, *J. Alloys Compd.*, 2017, **727**, 792–820.
49 K. Nithya and S. Kalyanasundharam, *OpenNano*, 2019, **4**, 100024.
50 N. Babayevska, Ł. Przysiecka, I. Iatsunskyi, G. Nowaczyk, M. Jarek, E. Janiszewska and S. Jurga, *Sci. Rep.*, 2022, **12**, 8148.